

INTERNATIONAL CONFERENCE ON ADVANCES IN MECHANICAL ENGINEERING ISTANBUL 2015 - ICAME'15
13-15 May 2015, Yildiz Technical University, Istanbul, Turkey

INVESTIGATION OF CAVITATION AROUND DISK AND CONICAL CAVITATORS USING DIFFERENT SETS OF TURBULENCE AND CAVITATION MODELS

Mohammad-Reza Pendar
MSc Student
HPC Lab, Dept. of Mechanical Eng.,
Ferdowsi University of Mashhad, Iran

***Ehsan Roohi**
Assistant Professor,
HPC Lab, Dept. of Mechanical Eng.,
Ferdowsi University of Mashhad, Iran

Keywords: cavitator, supercavitation, Volume-of-Fluid (VOF), mass transfer model, OpenFOAM
**Corresponding author: Ehsan Roohi, Phone: +98 (51) 38805136, Fax: +98 (51) 38763304*
E-mail address: e.roohi@ferdowsi.um.ac.ir

ABSTRACT

In this work, we investigated cavitation around two kinds of 3D cavitators, disk and conical cavitators, over a wide range of cavitation numbers. Dynamic and unsteady behaviors of cavitation is simulated under the framework of the OpenFOAM. The volume of fluid (VOF) method is applied to track the interface of liquid and vapor phases. The main innovation in this work is providing a detailed comparison of two kinds of turbulence models; LES, $k-\omega$ SST and two different types of mass transfer models; Kunz and Sauer. Discussions on the boundary layer separation, re-entrant jet behavior, cavity cloud shape/length and diameter, streamline vortices, pressure/volume fraction and velocity contours in very low cavitation numbers are reported. Our numerical results are compared with the experimental data and a wide set of analytical relations for the cavity characteristics that suitable accuracy was observed. Our results indicate that the most accurate solutions could be obtained if we employ LES turbulence modeling with the Kunz mass transfer model.

INTRODUCTION

Cavitation can be defined as formation of vapor bubbles within a liquid when the pressure locally drops below the saturated vapor pressure. Cavitation, as a critical phenomenon, has been considered in the past by many researchers. It could appear over most underwater vehicles such as high speed torpedoes, hydrofoils and propellers. After the cavity formation, cavity is usually exposed to unsteady dynamic behavior such as the periodic shedding of the cavity cloud. The collapse of the vapor cloud may cause loud, noise and erosion

damage. Study of cavitating flow behind cavitators has usually been of interest for many researchers. Three important points must be considered regarding the simulation of a 3-D cavitation: selection of an appropriate mass transfer model, a solution technique for the advection equation of the free surface and an appropriate turbulence model. Volume of fluid (VOF) technique could be employed to solve the advection equation of the volume fraction and predict the cavity interface accurately. Different approaches such as "large eddy simulation (LES)" and $k-\omega$ SST have been recently utilized to implement turbulence effects on cavitating flow. The benefit of the LES is that it can capture the details of small-scale flow structures in cavitating flow. Passandideh-Fard and Roohi [1] considered transient 2D/axisymmetric simulations of cavitating flows behind the cone and disk cavitators by using a modified VOF technique in a wide range of cavitation numbers. Nouri et al. [2] used VOF method to simulate the developing cavitation behind a cavitator by using the Kunz cavitation model and LES turbulence model. They compared their results with the experimental data. Accurate results show the ability of their combination cavitation and turbulence models to predict cavity characteristics. Guo et al. [3] simulated the cavitating flow around an underwater projectile with natural and ventilated cavitation based on the homogeneous equilibrium flow model, a mixture model for transport equation and a local linear low-Reynolds-number $k-\omega$ turbulence model. They showed that the morphology of cavity with much details. Shang [4] simulated cavitation around the cylindrical submarine. They used $K-\omega$ SST for turbulence model, VOF method for interface between the liquid and vapor phases and the Sauer for mass transfer

model were employed to capture the cavitation mechanisms within wide ranges of cavitation numbers from 0.2 to 1.0.

Yu et al. [5] simulate dynamic behaviors of cavitation in a 3-D projectile at cavitation number $\sigma=0.58$ based on LES methodology, $k-\mu$ transport equation and VOF description with the Kunz model for mass transfer. Baradaran-Fard and Nikseresht [6] simulated unsteady 3-D cavitating flows around a cone and disk cavitor. RANS (Reynolds Average Navier Stokes) equations and an additional transport equation for liquid volume fraction are solved by using a finite volume approach through the SIMPLE (Semi-Implicit Method for Pressure Linked Equations) algorithm. For implementation of the turbulent flow, $k-\omega$ SST model was used. The results are in good agreement with experimental data and analytical relations. Park et al. [7] simulate a high-speed super-cavitating flow around a 2-D symmetric cavitor and hemispherical head-form body e with using an unsteady Reynolds-averaged Navier–Stokes equations solver based on a cell-centered finite volume method. The computed result compared with an analytic solution and numerical results using a potential flow solver. Fairly good agreement was observed in the three-way comparison. Yu et al. [8] simulate dynamic behaviors of cavitation in a 3-D projectile at cavitation number $\sigma=0.58$ based on LES methodology, $k-\mu$ transport equation and VOF description with the Kunz model for mass transfer. Evolution of cavitation in simulation is consistent with the experiment.

In this research, we validate the ability of the open source package of OpenFOAM to simulate cavitation and supercavitation flow behind a conical cavitor that experimental and analytical data are widely available. Volume of fluid (VOF) technique is employed to track the interface of liquid and vapor phases, we use both of the LES and $k-\omega$ SST turbulence models to simulate cavitating flows behind the disk. We compared Kunz and Sauer mass transfer models.

GOVERNING EQUATIONS

In this work the interface between the liquid and vapor phases is captured by the volume of fluid (VOF) method [9]. Kunz et al. [10] proposed a semi-analytical cavitation model as follows:

$$\frac{\partial \gamma_g}{\partial t} + \vec{\nabla} \cdot (\gamma_g \vec{v}) = \frac{C_{prod} \rho_g \text{Min}(P - P_g, 0) \gamma_g}{\rho_l (0.5 \rho_l u_{\infty}^2) t_{\infty}} - \frac{C_{dest} (1 - \gamma_g) \gamma_g^2 \text{Max}(P - P_g, 0)}{\rho_l t_{\infty} |P - P_g|} \quad (1)$$

Another mass transfer model was developed by Schnerr and Sauer [11] as follows:

$$\frac{\partial \gamma_g}{\partial t} + \vec{\nabla} \cdot (\gamma_g \vec{v}) = \frac{\rho_g \rho_l}{\rho} (1 - \gamma_g) \gamma_g \frac{3}{R_b} \sqrt{\frac{2 |P_g - P|}{\rho_l}} \quad (2)$$

Large eddy simulation (LES) turbulence approach is based on computing the large, energy-containing eddies that are resolved on the computational grid, whereas the smaller, more isotropic, sub-grid structures are modelled. In addition to the LES, the shear stress transport (SST) $k-\omega$ model [12] is utilized for turbulence modelling.

OpenFOAM VALIDATION

Before simulating cavitating flow behind a conical cavitor, we evaluate the accuracy of the OpenFOAM package in simulating incompressible turbulence, non-cavitating flow. Experimental investigation of unsteady flow behavior and vortex shedding behind a non-cavitating disk at different Reynolds numbers were reported in Ref. [13]. Here, we consider the flow at $Re_d = 2.8 \times 10^4$. Fig. 1-a shows the computational domain around the disk with a diameter of 0.1 m. This domain is considered according to the geometrical data of the water tunnel used in Ref. [13]. Fig. 1-b compares the experimental and numerical solution for the normalized velocity contour behind the disk. As the figure shows, suitable agreement is observed, especially for velocity contours behind the disk. Additionally, the Strouhal number calculated from the numerical simulation was around 0.14, which is quite close to the experimental data for this Reynolds number reported in Ref. [13].

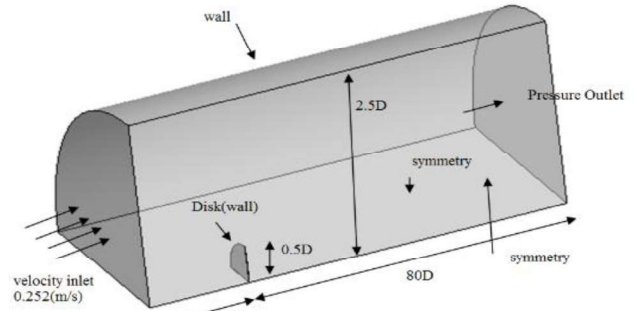


Fig 1-a: Computational domain around the disk considered for non-cavitating flow validation.

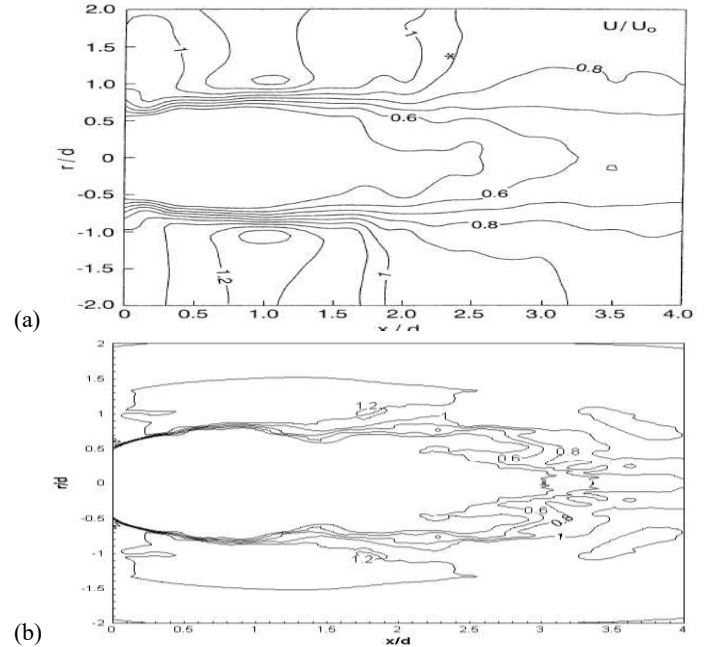


Fig 1-b: Comparison of the normalized velocity contour behind a vertical disk; a: Experiment picture from Ref. [13] b: current numerical simulation at a typical time step, $Re_d = 2.8 \times 10^4$.

SIMULATION SET-UP

The computational domain and boundary conditions for a conical cavitator are shown in Fig 2. The conical cavitator is placed at the center of the domain. As the geometry is not complex, we used structured quadrilateral meshes. Mesh resolutions near the body and close regions of the cavity cloud is higher than other region. Meshes are refined in both axial and radial directions to obtain cavitation characteristics accurately. the diameter of cone cavitator is $D=0.8284$ m. The computational domain is $120D$ in length (the length behind the cavitator length is $100D$ and distance in front of the cavitator is $20D$) and $52D$ in height. The boundary conditions are as illustrated in Fig 2. Two non-dimensional number: Reynolds ($Re = \rho U_{\infty} D / \mu$) and cavitation numbers ($\sigma = (P_{\infty} - P_g) / 0.5 \rho U_{\infty}^2$) are considered. For the conical cavitator, Reynolds numbers are 5×10^5 and 7×10^5 for $\sigma > 0.02$ and $\sigma = 0.02$, respectively. We considered the geometry as three-dimensional although both of geometries are axisymmetric, and the inflow conditions are steady; however, the flow is three-dimensional and unsteady due to the vortex shedding over the body at the investigated Reynolds numbers. Accuracy of results strongly depends on the mesh size near the body and especially around the cavity closure regions. In the other word, since the interaction between the near body flow and cavity is crucial; the mesh near the wall of a test body should be well refined. Figure 2-c shows that there is a dense mesh at the length of $L=30D$ and $60D$ for cavitation numbers $\sigma > 0.07$ and $\sigma = 0.02$ respectively. The grid size is progressively increased in the other regions, where the variations of flow proportion are small. This technique helps to save the computational cost and decrease the total cell numbers.

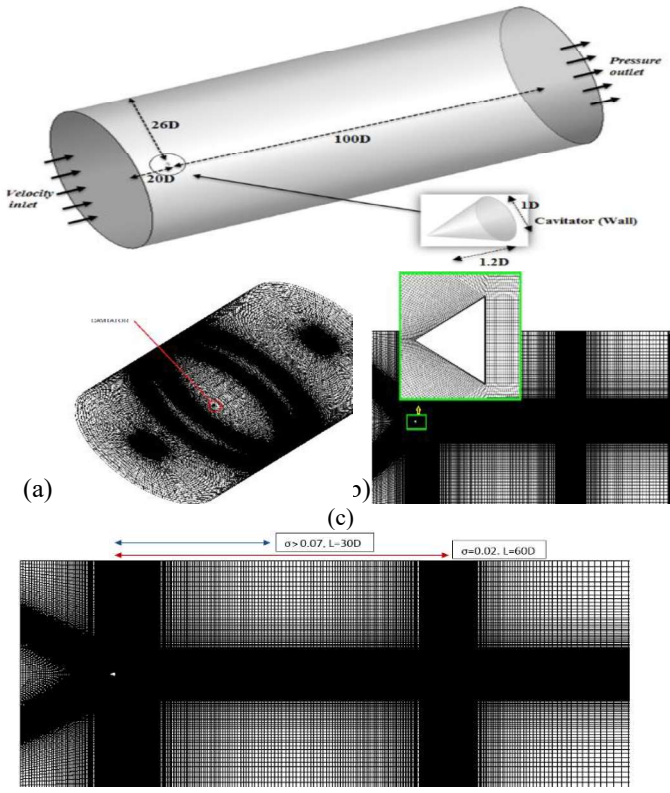


Fig 2: Computational domain and boundary conditions.

Table 1 compares simulation results for conical cavity parameters (length and diameter) obtained using different grid sizes with the analytical data. The grid used for $\sigma > 0.07$ cases are relatively coarse compared to those used for $\sigma = 0.02$. From table 1, it is observed that Grid 2 (which is 1×10^6 cells for $\sigma > 0.07$ and 2.4×10^6 cells for $\sigma = 0.02$) provides close solutions for predicting different characteristic of the cavity behind the conical cavitator. Therefore, we performed our simulations using Grid 2. The maximum values of y^+ was 241 and the mean values of y^+ was 8.59 for $\sigma = 0.02$ in conical cavitator case, respectively. For $30 < y^+ < 300$ at most positions, i.e., adjacent to the body region, OpenFOAM uses wall functions.

Table 1: Effect of different grid sizes on the cavity length/cavitator diameter and cavity diameter/cavitator diameter behind the cavitator.

| Mesh for $\sigma > 0.07$ | Cell number ($\times 10^6$) | L _{cavity} /d _{cavitator} | | D _{cavity} /d _{cavitator} | |
|--------------------------|-------------------------------|---|--------------------|---|--------------------|
| | | Simulation (LES/Sauer) | Reichardt's Theory | Simulation (LES/Sauer) | Reichardt's Theory |
| Grid1 | 0.75 | 15.21 | 13.19 | 2.20 | 2.19 |
| Grid2 | 1 | 12.20 | 13.19 | 1.96 | 2.19 |
| Grid3 | 1.5 | 13.01 | 13.19 | 2.20 | 2.19 |

| Mesh for $\sigma = 0.02$ | Cell number ($\times 10^6$) | L _{cavity} /d _{cavitator} | | D _{cavity} /d _{cavitator} | |
|--------------------------|-------------------------------|---|--------------------|---|--------------------|
| | | Simulation (LES/Sauer) | Reichardt's Theory | Simulation (LES/Sauer) | Reichardt's Theory |
| Grid1 | 1.8 | 67.25 | 55.53 | 4.30 | 3.96 |
| Grid2 | 2.4 | 61.46 | 55.53 | 3.91 | 3.96 |
| Grid3 | 3 | 59.42 | 55.53 | 3.92 | 3.96 |

Table 2 compares the required time to reach steady state condition for different models for two cavitation numbers for the cone cavitator. Simulations were performed in parallel using 4 and 12 cores of Intel® Core™ i7-2600K CPU equipped with 16 GB memory RAM in $\sigma = 0.07$ and 0.02 , respectively. In these simulations, the calculation is performed in a manner that Courant number in the computational domain does not surpass 0.175 for $\sigma = 0.07$ and 0.09 for $\sigma = 0.02$.

Table 2: Details of the computational cost of investigating test cases.

| | Turbulence and mass model | Steady Time (ms) | Run Time (hours) |
|--|---------------------------|------------------|------------------|
| $\sigma = 0.07$ Courant= 0.175 Grid2 Core number= 4 | K- ω SST/Sauer | 184 | 42 |
| | K- ω SST/Kunz | 180 | 46 |
| | LES/Sauer | 120 | 35 |
| | LES/Kunz | 104 | 43 |
| $\sigma = 0.02$ Courant= 0.09 Grid2 Core number= 12 | K- ω SST/Sauer | 450 | 58 |
| | LES/Sauer | 433 | 79 |

Table1 shows the initial and boundary condition for k and ω .

Table 1: initial and boundary condition for k and ω

| k | | |
|----------|-----------------|-------|
| boundary | type | value |
| disk | kqRWallFunction | 0.004 |
| outlet | inletOutlet | 0.004 |
| inlet | fixedValue | 0.004 |

| ω | | |
|----------|-------------------------------------|-------|
| boundary | type | value |
| disk | omegaWallFunction | 77200 |
| outlet | zeroGradient | ----- |
| inlet | turbulentMixingLengthFrequencyInlet | 77200 |

Our numerical solution follows the PIMPLE algorithm. Fig. 3 depicts PIMPLE flowchart, which is a merged PISO-SIMPLE algorithm to solve the pressure-velocity coupling. The PIMPLE algorithm enables a more robust pressure-velocity coupling by coupling a SIMPLE outer-corrector loop with a PISO inner-corrector loop. This algorithm shows a better numerical stability for larger time-steps or higher Courant number compared to PISO. Typically PISO and SIMPLE iterations are required per time step. Here, we employed two PISO and one SIMPLE iteration.

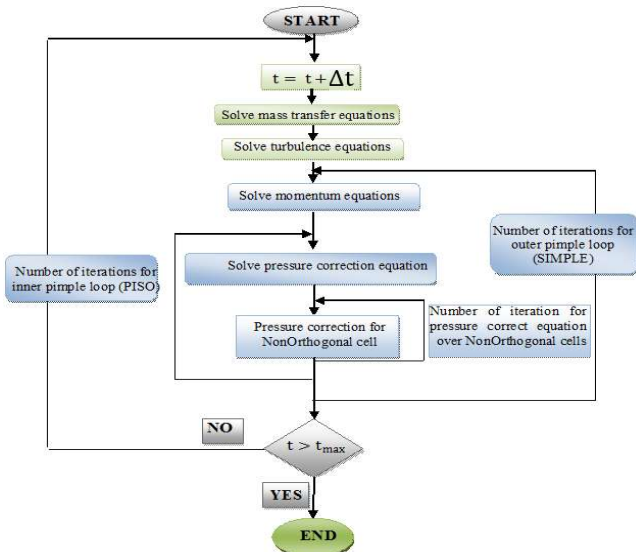


Figure 3: PIMPLE flowchart

Figure 4 shows the residuals convergence history of the liquid volume fraction (alpha) and pressure (p) for the five last time steps for a typical test case at $\sigma = 0.07$. The iterative convergence of unsteady flow problems depends on time step and the number of iterations per time step. Residual of each parameter is defined as the normalized difference between the current and the previous value of that parameter. Residuals increase at the beginning of each time step and then drop by two to three orders of magnitude.

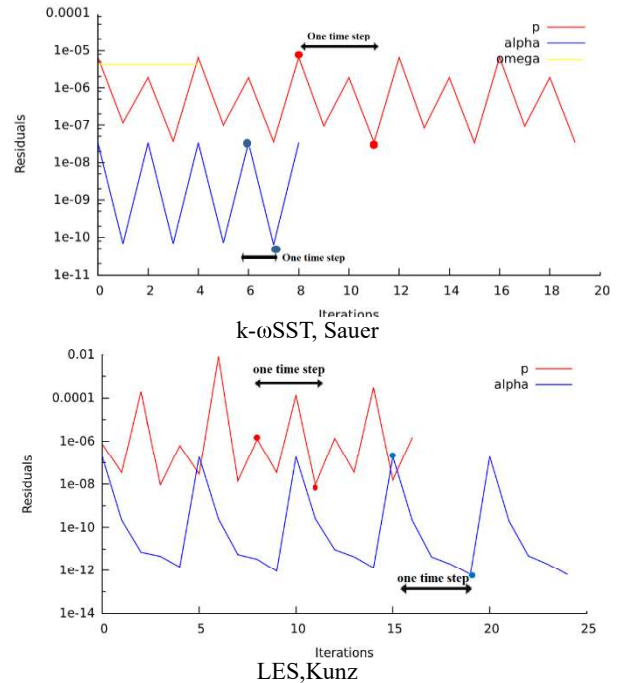


Figure 4: Convergence of residuals for five last time steps at $\sigma = 0.07$.

RESULTS AND DISCUSSION

Fig. 5 illustrates a 3D view of the cavitating flow over the conical cavitator in $\sigma = 0.07, 0.02$ obtained using different turbulence and mass transfer models. The cavity has a uniform shape and has a steady behavior. All models show nearly the same length and diameter of the cavity clouds.

